Quantum Monte Carlo simulations of the degenerate single-impurity Anderson model

J. Bonča* and J. E. Gubernatis
Theoretical Divison and Center for Nonlinear Studies, Los Alamos National Laboratory, Los Alamos, New Mexico 87545
(Received 19 January 1993)

We present results of quantum Monte Carlo simulations of the degenerate, single-impurity, Anderson model. Using maximum-entropy methods, we performed the analytic continuation of the imaginary-time Green's functions produced by these simulations to obtain their real-frequency, single-particle, spectral densities for degeneracies of $N=2$, 4, and 6. Incorporating higher degeneracies into the model enables us, on the one hand, to compare Monte Carlo results with the self-consistent large-N approximation (NCA) and numerical-renormalization-group calculations (NGR) and, on the other hand, to bring the models closer to the physical systems. The low temperatures reached in our calculations are comparable to, or even lower than, the corresponding Kondo temperatures. The NCA and NRG calculations were found to show qualitatively good agreement with our results: the Kondo temperature increases with increasing degeneracy, and the amplitude of the side peaks in the spectral density decreases as degeneracy increases while the half-width of these peaks increases.

I. INTRODUCTION

In spite of the fact that the single-impurity Anderson model[1] was first proposed 30 years ago as a model for the properties of dilute magnetic alloys, theoretical and numerical work on the model remains very active because it is one of the simplest paradigms for a system of strongly interacting electrons. Over the years, considerable progress has been made in understanding the properties of the model by several significant advances in analytic and numerical techniques. These techniques have sought to calculate various static and dynamic correlation functions to reveal the relevance of the model for such many-body phenomena as the Kondo effect, mixed valence fluctuations, and local magnetic-moment formation that are observed in dilute magnetic alloys.

Analytically, the exact solutions for ground-state properties of the spin-degenerate ($N=2$) and orbital-degenerate ($N>2$) versions of the model were found with the Bethe-ansatz technique.[2] The results for the spin-degenerate model confirmed and extended the prior work of Krishna-murthy, Wilkins, and Wilson,[3] who used the numerical-renormalization-group (NRG) technique to calculate various static properties of the spin-degenerate model. This numerical approach was, in turn, extended by Oliveira and co-workers[4,5] to the computation of ground-state dynamic properties of the model, first for the x-ray-absorption problem and then for the photoemission and photoabsorption problem.

Recently, Sakai, Shimizu, and Kasuya[6] used this method to calculate the ground-state spectral densities for the orbital-degenerate model. From the point of view of approximate theory, self-consistent large-N (NCA) expansions[7] provided the first extensive finite-temperature results both for the static and the dynamic properties of the model. The initial calculations, however, were restricted to the limit of an infinite interaction between two electrons occupying the same orbital state, thereby allowing only states with zero or single occupancy.

Although the main features of the spectral density function of the degenerate model, such as the position of the broad side peaks and the existence of a sharp resonance close to the Fermi energy, are likely well reproduced by different analytical and numerical methods, relative spectral weights and their temperature dependence often seem to be dependent on the underlying approximation. Therefore, there is a need for a method which calculates the spectral density function of the degenerate Anderson model at arbitrary interaction strength U, hybridization Γ, degeneracy N, and temperature T. In many respects, the quantum Monte Carlo method fulfills this need. Incorporating higher degeneracies into the model, on the one hand, enables a comparison of quantum Monte Carlo results with the NCA and numerical-renormalization-group calculations and, on the other hand, brings the calculations closer to physical systems. For example, a degeneracy of $N=6$ matches the degeneracy of a Ce impurity in a host with cubic symmetry and strong spin-orbit splitting. Moreover, in spite of numerous experimental and theoretical works in the field of dilute magnetic alloys, some disagreement still exists between theory and experiment, and even among different experimental groups.[8,9] Spectroscopic investigations are primarily done on ordered alloys and compounds, with the assumption that the single-impurity theory can be directly applied to these concentrated systems. The generally accepted belief is that the single-impurity model reproduces the main spectral features in Ce or Yb heavy fermion compounds;[8] however, recent studies by Joyce *et al.*[9] show features near $\omega=0$ that do not appear to scale with the Kondo temperature T_K or display the appropriate temperature dependence. These findings remain a puzzle.

In this paper, we will present calculations of the spectral properties of the degenerate Anderson model without the restriction of infinite U and zero temperature or with the concern about whether N is large enough for NCA approximations to be clearly appropriate. We will build

upon the work of Silver *et al.*,[10] who successfully obtained the single-particle spectral function for the spin-degenerate model from the imaginary-time Green's function calculated by quantum Monte Carlo simulations. A key point in their approach was the use of the method of Bayesian statistical inference, with the principle of maximum entropy, to regularize the numerical extraction of the spectral density for simulation data.

In particular, we will present spectral densities for the orbital-degenerate single-impurity Anderson model obtained by means of the quantum Monte Carlo method, proposed by Hirsch and Fye,[11] which we extended to higher degeneracies. In contrast to analytical and NRG approaches, this method enables us to treat exactly the localized impurity state coupled with an infinite sea of conducting electrons. The only systematic error comes from discretizing the imaginary time while evaluating the path integral representing the partition function. With this method, we reached temperatures below the Kondo temperature T_K. As a direct result of the method, we first obtain the impurity part of the many-body, imaginary-time Green's function and then perform the analytic continuation, using the maximum-entropy method, to obtain the impurity contribution to the spectral function.

This paper is organized as follows: In Sec. II, we briefly discuss the model and some of the relevant sum rules appropriate to it. In Sec. III, we summarize the quantum Monte Carlo and maximum-entropy methods. For the quantum Monte Carlo algorithm, we generalize Hirsch and Lin's application of the Hirsch-Fye algorithm for a doubly spin-degenerate case to a model with arbitrary degeneracy. In Sec. IV, we present results. Our basic result affirms the existence of universality in the presence of degeneracy greater than or equal to 2. Our calculated spectral densities provide benchmarks for approximate methods and for model appropriateness relative to experiment. We conclude with suggestions for future work in Sec. V.

II. MODEL AND SUM RULES

We treated the following form of the degenerate Anderson model:[7]

$$\begin{aligned} H&=H_0+H_1 \ , \\ H_0&=\sum_{km}\epsilon_k n_{km}+\sum_{km}V_{km}(c_{km}^{\dagger}f_m+f_m^{\dagger}c_{km})+\sum_m \epsilon_m n_m \ , \\ H_1&=\tfrac{1}{2}\sum_{m,m'}U_{mm'}n_m n_{m'} \ , \end{aligned} \tag{1}$$

where $c_{km}^{\dagger}$ creates a state in the conduction band with the energy ϵ_k in the channel m, $f_m^{\dagger}$ creates an orbital state m at the impurity site with the unrenormalized energy ϵ_m, and n_{km} and n_m are the number operators for the conduction band and orbitals at the impurity site. V_{km} represents hybridization between the conduction band and the localized impurity states. We will assume that the conduction band is infinitely wide and structureless; therefore V_{km} is neither energy nor channel dependent. This assumption leads to the simple relation for the impurity-level half-width $\Gamma=\pi N(0)V$, where $N(0)$ is the energy density of states per spin at the Fermi energy. The symmetric matrix $U_{mm'}$, with the additional condition $U_{mm}=0$, represents the Coulomb repulsion between two electrons occupying different orbitals at the impurity site. Furthermore, we associate the channel index m with the magnetic quantum number $m\equiv m_j$ since we want to model systems with strong spin-orbit coupling, such as Ce impurities in a metal. In particular, the low-lying multiplet in Ce has a total angular momentum $j=\frac{5}{2}$ and therefore a degeneracy $N=2j+1=6$, which represents the highest degeneracy reached in our calculations.

In the special case, when $\epsilon_m=\epsilon_f$ does not depend upon m and $U_{mm'}=U$ does not depend on m and m', the Hamiltonian (2) has particle-hole symmetry when $\epsilon_f=-(N-1)U/2$. In this case, the parameter space is limited to the values of U and Γ. In the asymmetric case, where we have an additional parameter ϵ_f, the particle-hole transformation preserves H if ϵ_f is replaced by $-[\epsilon_f+(N-1)U]$. Thus it is sufficient to study a limited-parameters space where $\epsilon_f>-(N-1)U/2$.

Various basic properties of this model have been determined analytically and numerically. Schlottman[12] solved the Bethe-ansatz equations in the limit $U\rightarrow\infty$ and obtained exact solutions for the occupation number, charge and spin susceptibility, and resistivity. In the case where the Anderson Hamiltonian can be transformed to the Coqblin-Schrieffer Hamiltonian, he also estimated the low-energy scale defining the Kondo temperature T_K.

Lin and Hirsch[13] studied the static susceptibility and local-moment formation of a doubly degenerate parametrization of the model by a Monte Carlo simulation technique. They chose $N=4$, assumed $U_{mm'}=U$, but grouped the four values of ϵ_m into two groups of doubly degenerate state, i.e., they took $\epsilon'\equiv\epsilon_1=\epsilon_2$ and $\epsilon''\equiv\epsilon_3=\epsilon_4$. To mimic the crystal-field splitting of the impurity states of a transition-series atom, they simulated the properties of the model for various values of $\Delta=\epsilon''-\epsilon'$. (Their model also incorporated the exchange interaction originally proposed by Anderson.) Their main finding was that the static magnetic susceptibility follows a universal curve as a function of T/T_K.[3]

We will mainly be concerned with the computation of the single-particle spectral density associated with the impurity state. Several important features of this function are known quite generally. The imaginary-time Green's function $G(\tau)$, which we will obtain using quantum Monte Carlo simulation procedures, is directly connected to the spectral function $A(\omega)$ through the following relation:

$$G(\tau)=\int_{-\infty}^{+\infty}d\omega\frac{e^{-\tau\omega}}{1+e^{-\beta\omega}}A(\omega) \ , \tag{2}$$

where β is the inverse temperature. In the case of particle-hole symmetry, the Green's function obeys the relation $G(\tau)=G(\beta-\tau)$ and therefore $A(\omega)$ is an even function of frequency. Furthermore, $A(\omega)$ obeys the following sum rules:

$$\int_{-\infty}^{+\infty}d\omega\ A(\omega)=1 \ , \tag{3}$$

$$\int_{-\infty}^{+\infty} d\omega f(\omega) A(\omega) = \frac{\langle n_f \rangle}{N} , \tag{4}$$

$$\pi\Gamma A(0)|_{T=0} = \sin^2 \left[\frac{\pi \langle n_f \rangle}{N} \right] \Bigg|_{T=0} , \tag{5}$$

where $f(\omega)$ is the Fermi function and $\langle n_f \rangle$ represents the average occupancy at the impurity site. The first equation (3) follows from the general properties of spectral functions.[14] The second equation follows from (2), (3), and our choice of convention to express the discontinuity in the Green's function at equal times.[15] The third equation (5), a representation of the Friedel sum rule, was derived for the Anderson impurity model by Langreth[16] and is valid only at $T=0$. Even so, (5) still provides useful information about simulations which are done at finite temperatures. Specifically, the extent to which our results satisfy this relation is a qualitative measure of the extent to which the temperature of our simulation is above or below the Kondo temperature. It also reveals similar information about other approaches. As the degeneracy increases, the relation begins to fail for the NRG results which are done at $T=0$. This breakdown is a consequence of the inability to store in the computer's memory sufficient energy states for the method to achieve its full potential.[6]

Using the NRG, Sakai, Shimizu, and Kasuya[6] calculated spectral functions for degeneracies up to $N=5$. In the case of particle-hole symmetry (the symmetric case), they found that the width of the $\omega=0$ peak (the Kondo resonance) decreases with increasing ratio U/Γ. In addition, they found that the width of the $\omega=0$ peak is always smaller than Γ, and that the shoulders of the central peak at small U/Γ transform into broad side peaks as U/Γ is increased. The side peaks correspond to excitations where an electron is being added or removed from the impurity level f. In the asymmetric case (the absence of particle-hole symmetry), in the case when the average electron occupancy $\langle n_f \rangle \sim 1$, they observed that for a given value of U the width of the central peak does not change significantly from the symmetric case, but again the shoulders on the central peak broaden both for $\omega>0$ [the bremsstrahlung isochromat spectroscopy (BIS) side of the spectrum] and for $\omega<0$ [the photoemission spectroscopy (PES) side] due to excitations from a singly to doubly occupied state ($f^1 \rightarrow f^2$) and from a singly to unoccupied state ($f^1 \rightarrow f^0$). The peak on the BIS side had a smaller width and carried larger spectral weight than the f^0 peak on the PES side.

Spectral functions calculated with the NCA,[7] because of the infinite-U assumption, show only two peaks: a broad peak due to $f^1 \rightarrow f^0$ excitations near the renormalized impurity energy ϵ_f with a half-width $\sim N\Gamma$ and height $\sim 1/(N^2\Gamma)$, and the Kondo resonance peak near $\omega=0$ with a half-width $\sim T_0/N$ and height $\sim 1/\Gamma$, where T_0 represents the low-temperature scale which is essentially a measure of magnetic excitations. There is no peak at large positive frequencies because U is infinity. Attempts have been made to go beyond the NCA approximation to include doubly occupied sites. For $N=2$, Holm and Schönhammer[17] introduced "heavy bosons" to represent the doubly occupied states. An attempt to include finite values of U for arbitrary degeneracies was made by Keiter and Quin.[18] They showed that inclusion of doubly occupied states leads to a coupled system of integral equations for vertex functions, which they solved numerically in a simplified form. Besides the peak at ϵ_f, another peak now exists at $\epsilon_f + U$. Their results show that with increasing U, the height of this peak increases and its width narrows. Lowering the temperature has almost no effect on peaks at ϵ_f and $\epsilon_f + U$, while the central peak close to $\omega=0$ becomes sharper.

III. METHODS

A. Quantum Monte Carlo

The Monte Carlo method we used was originally developed to treat the single-impurity, spin-degenerate ($N=2$) Anderson model[11] and was later generalized to treat the doubly spin-degenerate Anderson model.[13] Here we present the method for arbitrary degeneracy.

Dividing the imaginary-time scale into L discrete time intervals $\Delta\tau=\beta/L$ allows us to write a path-integral formulation for the partition function as

$$Z = \mathrm{Tr} e^{-\beta H} = \mathrm{Tr} \prod_{l=1}^{L} e^{-\Delta\tau H} \simeq \mathrm{Tr} \prod_{l=1}^{L} e^{-\Delta\tau H_0} e^{-\Delta\tau H_1} , \tag{6}$$

where we used a Trotter approximation to separate the exponents since H_0 and H_1 (2) do not commute. Next, we transform the electron-electron interaction part of the Hamiltonian H_1 into a noninteracting one by introducing discrete Hubbard-Stratonovich variables.[11] In the case of general degeneracy, this transformation at time step l is

$$\begin{aligned} &\exp(-\Delta\tau U_{mm'} n_m n_{m'}) \\ &\quad = \tfrac{1}{2} \exp[-\Delta\tau U_{mm'}(n_m + n_{m'})/2] \\ &\qquad \times \sum_{S^l_{mm'}=\pm 1} \exp[S^l_{mm'} J_{mm'}(n_m - n_{m'})] , \end{aligned} \tag{7}$$

where $\cosh(J_{mm'}) \equiv \exp(\Delta\tau U_{mm'}/2)$ and auxiliary fields $S^l_{mm'}$ form an antisymmetric matrix. The Hubbard-Stratonovich transformation enables us to take the trace over fermionic degrees of freedom exactly for a fixed configuration of the auxiliary fields $\{S\} \equiv \{S^1_{mm'}, S^2_{mm'}, \ldots, S^L_{mm'}\}$. The partition function (6) becomes

$$Z = \mathrm{Tr}_S \prod_{m=1}^{N} \det O_m(\{S\}) , \tag{8}$$

where O_m is a matrix of dimension $(N_k+1)L \times (N_k+1)L$, with N_k being the number of k vectors of the conduction electrons. The matrix elements of O_m are

$$\begin{aligned} &(O_m)_{l,l} = 1 , \\ &(O_m)_{l,l-1} = e^{-\Delta\tau K} e^{V_m^{l-1}} (1 - 2\delta_{l,1}) , \\ &(O_m)_{l,l'} = 0 \quad \text{otherwise} , \end{aligned} \tag{9}$$

where K represents the noninteracting part of the Hamil-

tonian in Eq. (2). The potential V_m^l, which couples to the orbital degrees of freedom, is a diagonal matrix and depends on the auxiliary fields which act only at the impurity site,

$$V_m^l = \sum_{m'} S_{mm'}^l J_{mm'} |f\rangle\langle f| \ . \tag{10}$$

The desired one-particle Green's function is the inverse of the O matrix: $G_m = O_m^{-1}$. Using Dyson's equation, we can connect different Green's functions corresponding to different potentials produced by different configurations of Hubbard-Stratonovich fields

$$G'_m = G_m + (G_m - I)(e^{V'_m - V_m} - I)G'_m \ . \tag{11}$$

We start the Monte Carlo calculation with the Green's function where all auxiliary fields are zero. We do this calculation exactly for an infinite, structureless conduction band. Then, for each time slice, we generate an arbitrary configuration of auxiliary fields $\{S\}$ and calculate the interacting Green's function G' using the Dyson equation (11). With this Green's function, we then begin the Monte Carlo steps in which we flip (change the sign) each component of the auxiliary fields $S_{mm'}^l$ while conserving the asymmetry of $S_{mm'}^l$. In this process, we use the Metropolis algorithm to determine whether we accept the flip. If we accept, we update the Green's function for the new configuration of auxiliary fields using (11), and need only to consider its components among impurity orbitals since the interaction is only among these states.

The method produces the Green's function as a function of τ as its natural product. For a given configuration of Hubbard-Stratonovich fields, this is the exact Green's function, within the systematic error caused by the Trotter approximation, because the Hubbard-Stratonovich transformation converts the interacting problem into a noninteracting problem which is, of course, solvable. This conversion also means that various thermodynamic averages are directly computable from the Green's function by use of Wick's theorem. Averaging these quantities over many Hubbard-Stratonovich configurations restores the interactions.

B. Maximum entropy

Using Eq. (2), we seek to determine the spectral function at a large number of discrete frequencies $A(\omega_i)$, called the image, from the calculated Green's function $G(\tau_l)$ at a smaller number of discrete imaginary-time values, called the data. This problem is also known as the analytic contribution problem because the dynamics defined on the imaginary-time axis is used to determine real-time dynamics. There are several difficulties associated with this problem: the Green's function is almost insensitive to changes in $A(\omega_i)$ at large frequencies due to the exponentially small kernel. This insensitivity makes the problem extremely ill posed; that is, small variations in the values of $G(\tau_l)$ can lead to major variations in the solution $A(\omega_i)$. With $G(\tau_l)$ being determined by a Monte Carlo procedure, variations in the data (noise) are a fact. Furthermore, the number of data is smaller than the desired number of image points $A(\omega_i)$; thus we cannot solve the problem exactly. There is also a practical limit to the number of $G(\tau_l)$ values that can be produced. Increasing their number by decreasing $\Delta\tau$ for a fixed β reaches a point where the difference between successive values of $G(\tau_l)$ becomes smaller than the accuracy of the calculation, and hence the production of new information ceases.

Bayesian statistical inference, with the principle of maximum entropy, yields procedures that enable the analytic continuation and represent a major improvement over a constrained least-squares method.[19] The approach is based on probability theory and relies on the specification of probability and conditional probability functions connected by Bayes's theorem. The principle of maximum entropy uses the *a priori* knowledge that the spectral density is non-negative and is normalizible (satisfies a sum rule), and it enters the process by specifying the prior probability of the image, namely

$$P[A] \propto e^{-\alpha S} \ , \tag{12}$$

where

$$S = \sum_i [A_i - m_i - A_i \ln(A_i/m_i)] \ . \tag{13}$$

The function m_i is called the model and it sets the zero of the entropy S. This approach is quite different than the constrained least-squares method, which would use the non-negativity and sum rule as constraints on the solution and then be forced to determine the associated Lagrange multipliers in an *ad hoc* manner.

Our results are calculated from[19,20]

$$\langle A \rangle = \int d\alpha \, P[\alpha|G,m] A(\alpha) \ , \tag{14}$$

where the conditional probability function $P[\alpha|G,m]$ is found by using Bayes's theorem. Details are given elsewhere,[19] but the main ingredient, besides (12), is the choice of the likelihood function

$$P[G|A] \propto e^{-\chi^2/2} \ , \tag{15}$$

where χ^2 is the least-squares function

$$\chi^2 = \tfrac{1}{2} \sum_{ik} \left[G_i - \sum_j K_{ij} A_j \right] C_{ik}^{-1} \left[G_k - \sum_j K_{kj} A_j \right] \ , \tag{16}$$

with K_{ij} being the kernel from the Eq. (2) and C_{ij} the covariance matrix[19] for the different τ components of $G(\tau_l)$.

The choice (15) of the likelihood function assumes that the data are statistically independent and Gaussian distributed. These assumptions, which are implicit in a least-squares procedure, are not naturally satisfied. Promoting the consistency of the data with them was achieved by using large bins to reduce the correlations between binned measurements and a large number of bins to generate the Gaussian behavior. The large number of binned measurements also reduces the statistical error associated with the measurements. Because the covariance matrix is not diagonal and its eigenvalues span four to six orders of magnitude for this problem, the standard root-mean-square error estimate is meaningless. The number of bins calculated was found empirically to be the number needed, so the results did not change if this number was increased.

IV. RESULTS

In this section, we present results for the magnetic susceptibility and the spectral functions obtained by quantum Monte Carlo simulations for the degenerate Anderson model for the degeneracies $N=2$, 4, and 6. We used an energy scale in which the full width of the resonance equals unity, that is, $2\Gamma=1$. In the symmetric case, we will present calculations for three different on-site Coulomb repulsion strengths $U=2$, 3, and 4 in units of 2Γ. In the asymmetric case, we limit our calculations to the single value $U=4$ and follow the changes in the spectral functions due to changing the impurity energy ϵ_f.

We define the magnetic susceptibility as

$$\chi=\int_0^\beta d\tau\langle J_z(\tau)J_z(0)\rangle \ , \tag{17}$$

where J_z is

$$J_z(\tau)=\sum_{m=1}^{N}\left[m-\frac{N+1}{2}\right]n_m(\tau) \ . \tag{18}$$

The magnetic susceptibility (17) can be obtained from the Green's function using Wick's theorem

$$J_z(\tau)J_z(0)=\sum_{m,m'=1}^{N}\left[m-\frac{N+1}{2}\right]\left[m'-\frac{N+1}{2}\right] \times\{[1-G_m(0)][1-G_{m'}(0)] +\delta_{mm'}[\delta(\tau)-G_m(-\tau)]G_m(\tau)\} \ . \tag{19}$$

The choice of $\Delta\tau$ is most delicate since it introduces a systematic error. Relying on previous works,[19] we assumed that the value $\Delta\tau=0.125$ yields a systematic error which is smaller than the statistical error for $U\lesssim 4$ and $\Gamma\lesssim 0.5$. We reached temperatures as low as $KT=\frac{1}{16}$, in which case, for the assumed $\Delta\tau$, the number of time slices was $L=\beta/\Delta\tau=128$. We note that the computing time for the Hirsch-Fye algorithm scales as L^3N^2. In addition, due to the larger number of states, as the degeneracy N increases, equilibriating the simulation and producing statistically independent measurements becomes more difficult. These factors also increase the computation time proportionally to N; therefore, the total computational time scales as $(LN)^3$.

We estimated the covariance matrix in (16) from fluctuations about "bin averages."[19] Defining a sweep as making a Monte Carlo step for each m at all values of l, we need 10 000 sweeps in a bin and skipped nine sweeps between measurements to reduce correlations between measurements. Therefore, the number of measurements within a bin was 1000, and we calculated between 200 and 800 bins depending on degeneracy and temperature. At each measurement step, we calculated the one-particle Green's function and various static correlation functions such as the static magnetic susceptibility, average impurity occupancy, and local moment. From the static susceptibility, we find the Kondo temperature, and from the Green's function, we extract the spectral density using maximum-entropy methods. As the model in Eq. (13), we used a normalized Lorenzian, centered at $\omega=0$ with a width of 2Γ. The spectral density, when the data was good, was basically model independent.

All our calculations were performed on a cluster of 16 IBM/RS6000-560 workstations. Their combined performance was up to three times that of one CPU unit of a Cray Y-MP computer. Our computation times ranged from 1 h to three days.

A. Symmetric case

Figure 1 presents $T\chi$ for $N=4$ and 6 and for three different interaction strengths $U=2$, 3, and 4. All the $T\chi$ curves are divided by the high-temperatures limit $\langle J_z^2\rangle$. These renormalized curves follow the universal curves of Krishna-murthy, Wilkins, and Wilson[3] when temperatures $T\lesssim 0.5\Gamma$. We note that for the same choice of Γ, U, and T, the local moment regime[3] is much less pronounced than in the $N=2$ case.[19] Two factors contribute to this reduction: (a) because of a larger phase space, the effective hybridization is proportional to the

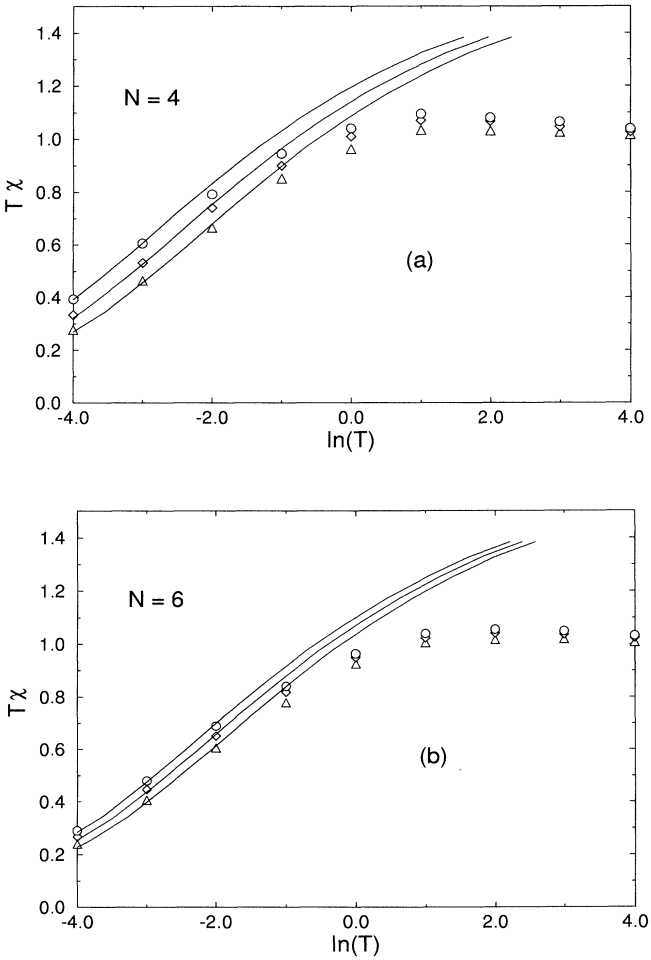

FIG. 1. The susceptibility $T\chi$ for (a) $N=4$ and (b) $N=6$, respectively, as a function of $\ln(T)$, and in the units of its high-temperature values $\frac{5}{4}$ and $4\frac{3}{8}$. The Monte Carlo results $U=2$, 3, and 4 are marked by △, ◇, and ○. The solid lines are the universal curves from Ref. 3. The estimated statistical errors are smaller than the height of the markers.

degeneracy $\bar{\Gamma}=N\Gamma$, and increased effective hybridization at higher N then reduces of the local-moment regime; (b) in the limit $\Gamma\to 0$, the ratio of the values of $T\chi$ in the local-moment regime and at the high-temperature limit decreases with degeneracy as $N/(N-1)$, so even in the case of strong local-moment formation the increase of $T\chi$ in the local-moment regime from the value at the high-temperature limit is strongly reduced at higher degeneracies.

In Table I, for $N=4$ and 6, we present Kondo temperatures T_K extrapolated from the susceptibility curves and T_K^* estimated from the semiempirical equation

$$T_K^*=\left[1+\frac{\pi\Gamma}{2U}\right]0.291\sqrt{U\Gamma}\exp\left[-\frac{\pi U}{4N\Gamma}\right]. \quad (20)$$

For $N=2$, Eq. (20), without the first prefactor, was derived by Haldane using the high-temperature perturbation theory.[21] The prefactor $(1+\pi\Gamma/2U)$ was obtained numerically by Silver *et al.*[10] We replaced the $\frac{1}{8}$ factor in the exponent of the original formula with the $1/4N$. The $1/N$ factor in the exponent can be obtained from strong-coupling theory and from $1/N$ calculations. We note that agreement between T_K and T_K^* is best for higher interaction strengths where the perturbation expansion of Haldane is expected to give reliable results. For $N=4$, we also found good agreement with the T_K calculated by Lin and Hirsch,[13] who investigated the spin-degenerate Anderson model with two degenerate orbitals.

Figure 2 presents spectral functions $\pi\Gamma A(\omega)$ at fixed $U=4$ and $T=0.125$, but for different degeneracies. We observe that the height of the central peaks at $\omega=0$ increases with N, which is in agreement with the increasing of the Kondo temperature T_K as a function of N. Here we recall that, according to the Friedel sum rule, when $T\ll T_K$ the renormalized spectral function at $\omega=0$ approaches unity.

The heights of the side peaks, representing transitions $f^{N/2}\to f^{N/2\pm 1}$, also scale with the degeneracy. We find surprisingly good agreement with analytical calculations by Zhang and Lee,[22] who predict that the heights scale as $\langle n_f\rangle/N^2$. In the particle-hole symmetric case, $\langle n_f\rangle=N/2$, so the Zhang-Lee results predict the ratios between the heights of the side peaks as being $1:\frac{1}{2}:\frac{1}{3}$, while from Fig. 2 we estimate 1:0.46:0.34. The $1/N$ calculations[7] predict that the width of the side peaks scales with the effective hybridization $\bar{\Gamma}=N\Gamma$. The side peaks in Fig. 2 share this tendency; however, at high degeneracies they merge with the Kondo peak, which prevents

TABLE I. The Kondo temperature T_K obtained from the universal behavior of the susceptibility curves presented in Fig. 1, and T_K^* calculated from the semiempirical Eq. (20).

	$N=4$		$N=6$	
U	T_K	T_K^*	T_K	T_K^*
4	0.108	0.102	0.164	0.173
3	0.139	0.138	0.186	0.205
2	0.174	0.185	0.211	0.240

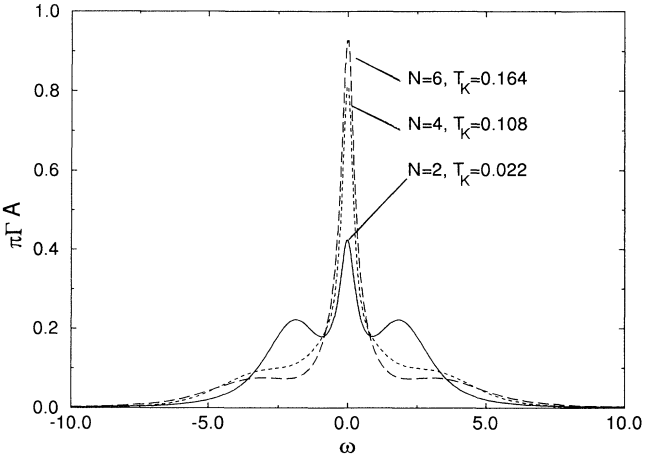

FIG. 2. The spectral densities $\pi\Gamma A$ in the symmetric case as functions of the frequency ω. The three curves differ only in degeneracy N. The values of the other parameters are $U=4$, $\Gamma=0.5$, and $T=0.125$. Also presented are the corresponding Kondo temperatures T_K.

further comparisons. In Fig. 3, we plot $\pi\Gamma A$ for $N=4$, $T=0.125$, and $U=2$, 3, 4. The central peak approaches unity with decreasing U since the Kondo temperature T_K increases. Moreover, when U decreases, the side peak shoulders merge with the Kondo peak.

One striking feature of the Anderson impurity model is the universal behavior of various physical properties if the temperature is scaled by the Kondo temperature. For the case of $N=2$, it has also been shown[19] that the spectral functions as functions of ω/T_K, when calculated at fixed T/T_K, follow a universal curve in the low-frequency regime. In Fig. 4, we present spectral func-

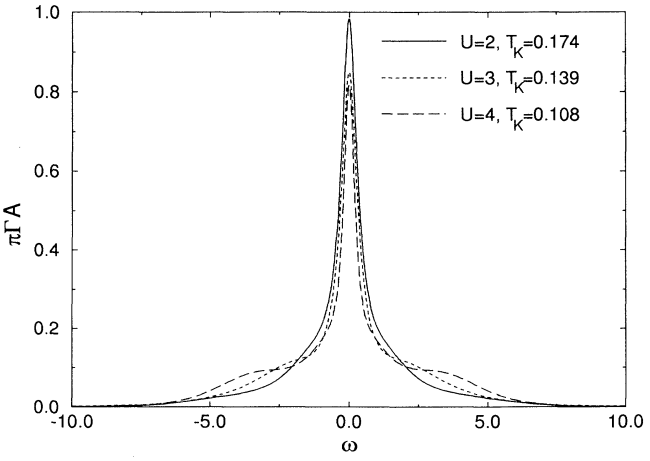

FIG. 3. The spectral densities $\pi\Gamma A$ for $N=4$ in the symmetric case as functions of the frequency ω. The three curves correspond to different interactions. The values of U are 2, 3, and 4. The values of the other parameters are the same as in Fig. 2.

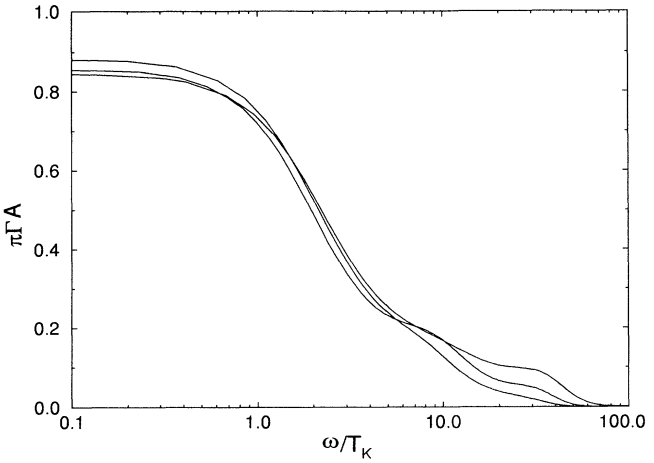

FIG. 4. The spectral densities $\pi\Gamma A$ as functions of ω/T_K calculated at $T/T_K=1.16$ and $N=4$ for $U=2$, 3, and 4.

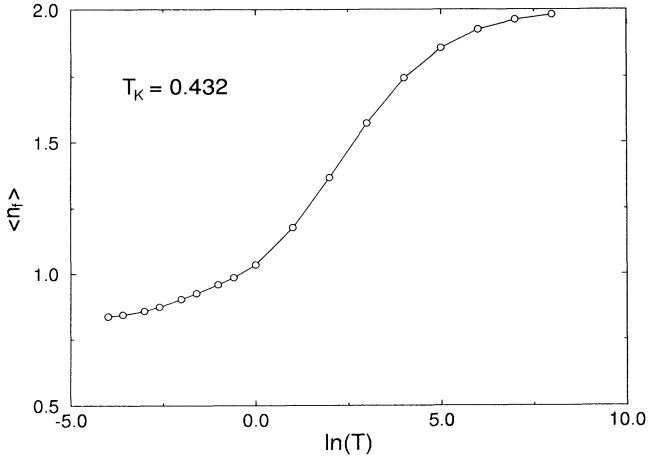

FIG. 6. The average impurity occupancy $\langle n_f \rangle$ as a function of $\ln(T)$ calculated at $N=4$, $U=4$, $\epsilon_f=-1$, and $\Gamma=0.5$. The Monte Carlo measurements are marked by open circles; the solid line is only a guide to the eye.

tions calculated at different interaction strengths $U=2$, 3, and 4, but fixed $T/T_K=1.16$. At small frequencies, when $\omega/T_K \lesssim 5$, the curves follow the same universal curve. Our calculations indicate that the universal behavior exists even among spectral functions calculated at different degeneracies. In Fig. 5, we present spectral functions of the systems $N=4$, $U=4$ with $T_K=0.108$, and for $N=6$, $U=4$ with $T_K=0.164$ calculated at a fixed ratio $T/T_K=2.98$. As seen from Fig. 5, the behavior in the low-frequency region $\omega/T_K \lesssim 10$ is universal within the statistical error.

B. Asymmetric case

Since the asymmetric case has an additional parameter ϵ_f, completely covering parameter space becomes difficult. To simplify things, we limited our calculations to $N=4$, $U=4$, and $\epsilon_f > -(N-1)U/2$. In Fig. 6, we show $\langle n_f \rangle$ as a function of $\ln(T)$ for $\epsilon_f=-1$. In this case, the lowest-lying impurity state is f^1. In the high-temperature limit, $\langle n_f \rangle$ approaches 2, since all impurity states are equally populated. As the temperature decreases, we observe a significant drop in $\langle n_f \rangle$ from its high-temperature value as the temperature becomes comparable to 20, the energy of the f^4 state. As the temperature further decreases, more impurity states with occupancy larger than unity depopulate, and in the low-temperature limit, because of hybridization, only states f^0 and f^1 contribute significantly to the ground state. This leads to $\langle n_f \rangle \sim 0.8$.

In Fig. 7, we present the magnetic susceptibility $T\chi$ as a function of $\ln(T)$ for the same set of parameters. As in the symmetric case, we divided $T\chi$ by its high-temperature value. In contrast to the renormalization-group work of Krishna-murthy, Wilkins, and Wilson[3] for $N=2$, where the susceptibility in the local-moment and

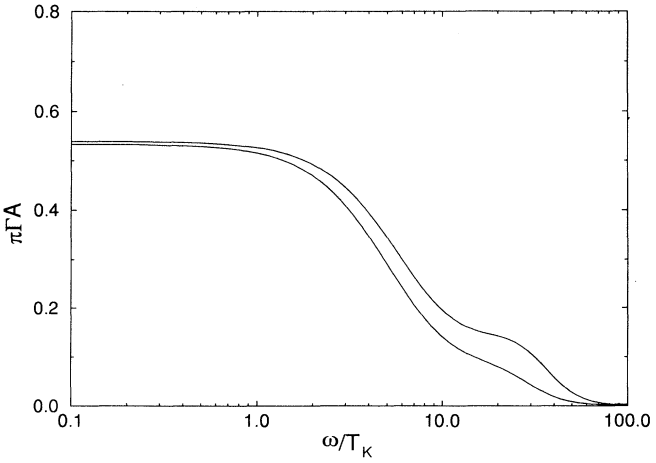

FIG. 5. The spectral densities $\pi\Gamma A$ as functions of ω/T_K calculated at $T/T_K=2.97$ and $U=4$ for $N=4$ and 6.

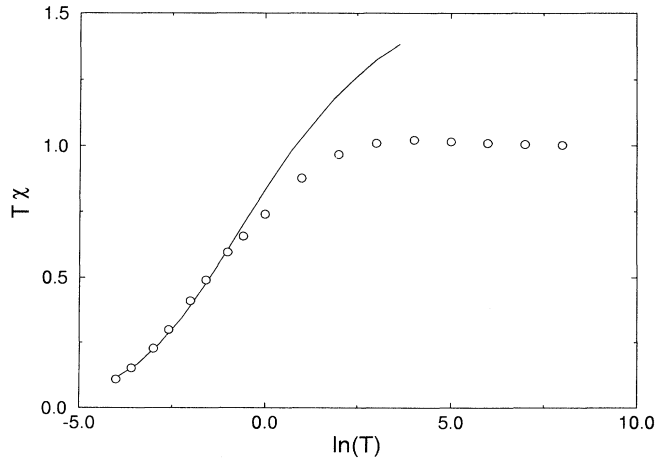

FIG. 7. The susceptibility $T\chi$ in units of its high-temperature value as a function of $\ln(T)$. The choice of parameters is the same as in Fig. 6.

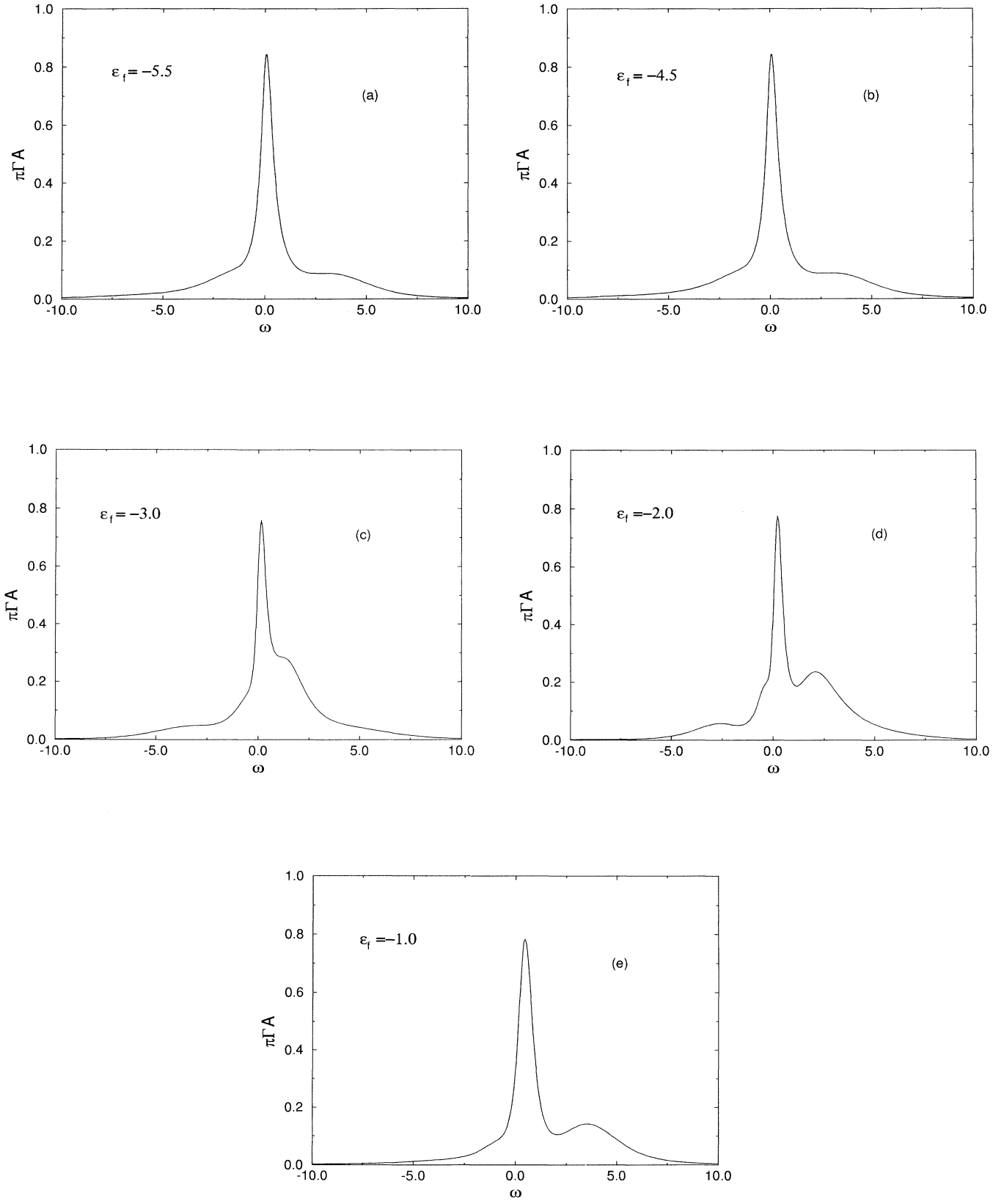

FIG. 8. The spectral densities $\pi\Gamma A$ in the asymmetric case as functions of the frequency ω calculated for $N=4$, $U=4$, $\Gamma=0.5$, $T=0.125$, and different impurity energies: $\epsilon_f=$(a) -5.5, (b) -4.5, (c) -3.0, (d) -2.0, and (e) -1.0.

mixed-valence regimes of the asymmetric case develops a pronounced cusp, we see only a small increase in $T\chi$ at intermediate temperatures. These differences, as in the symmetric case, are a consequence of higher degeneracy and stronger effective hybridization. At low temperatures, $T\chi$ again follows the universal curve.

In Figs. 8(a)–8(e), we plot the spectral functions for $N=4$, $U=4$, and $\epsilon_f=-5.5$, -4.5, -3, -2, and -1. For the given N and U, the value of ϵ_f in the symmetric case would be $\epsilon_f=-6$. As ϵ_f increases, the Kondo peak moves from its position at $\omega=0$ in the symmetric case to $\omega>0$. A rough estimate of this shift, value for $\langle n_f\rangle \gtrsim 1$, is $\Delta\omega=T_K(N-2\langle n_f\rangle)$.

In the asymmetric case, the comparison of the average occupancy $\langle n_f\rangle$ obtained directly and quite precisely from the Green's functions with that obtained from the spectral function using the sum rule (5) is a nontrivial test of the regularization method. A comparison of these values is presented in Table II and shows only a few percent difference.

In Fig. 8(a), we plot the spectral function of a system with only a slight asymmetry. In comparison with the spectral function for the equivalent symmetric case, presented in Fig. 2, we observe that the peaks in the PES and BIS sides of the spectrum, representing transitions $f^2\rightarrow f^1$ and $f^2\rightarrow f^3$, shift slightly to higher frequencies. This shift is a consequence of smaller energy differences $\Delta_{12}\equiv\epsilon_1-\epsilon_2=1.5$ between states f^2 and f^1 and the enhanced difference $\Delta_{32}=2.5$ between f^2 and f^3. This situation differs from the symmetric case where $\Delta_{12}=\Delta_{32}=2$. This shift is even more pronounced in Fig. 8(b), where Δ_{12} becomes of the order of hybridization, that is, $\Delta_{12}\approx-\Gamma$, which causes the peak in the PES side to merge with the Kondo peak and to become its shoulder. In contrast to Figs. 8(a) and 8(b), in Fig. 8(c) we have the singly occupied state f^1 as the state with minimum energy; therefore, the peaks in PES and BIS spectra represent transitions $f^1\rightarrow f^0$ and $f^1\rightarrow f^2$. On the PES side, we observe a small peak located approximately at $\omega\sim\Delta_{01}=3$. The peak on the BIS side is not well developed because its position at $\omega\sim\Delta_{21}=1$ is close to the origin. Thus we observe only a shoulder.

The choice of parameters in Fig. 8(d) is particularly significant for understanding the effects of higher degeneracy. The lowest-energy impurity state is f^1; however, at $\epsilon_f=-2$, the energy differences between f^1 and the next lowest states f^0 and f^2 are equal, that is, $\Delta_{01}=\Delta_{21}=2$. One could, therefore, naively expect the spectral function to be symmetric around the origin. Contrary to this expectation, the difference between peaks is significant and results in a different phase space for transitions $f^1\rightarrow f^0$ and $f^1\rightarrow f^2$.

TABLE II. A comparison of the average occupancies obtained from the Green's function $\langle n_f\rangle_G$ and from the spectral function $\langle n_f\rangle_A$.

ϵ_f	-5.5	-4.5	-3.0	-2.0	-1.0
$\langle n_f\rangle_G$	1.90	1.67	1.28	1.06	0.86
$\langle n_f\rangle_A$	1.89	1.67	1.31	1.14	0.92

V. CONCLUSIONS

Using the quantum Monte Carlo (QMC) technique, we calculated the magnetic susceptibility and the single-particle spectral density of the degenerate, single-impurity Anderson model for degeneracies $N=2$, 4, and 6 in the particle-hole symmetric case. We also presented results for the asymmetric case at $N=4$. We generalized the QMC method, originally developed for the spin-degenerate model by Hirsch and Fye, to arbitrary degeneracies. The spectral densities were extracted via analytic continuation from the imaginary-time Green's function, where the extraction was regularized using methods of Bayesian statistical inference with the principle of maximum entropy. Our results in general agree well with those obtained by the NCA and NRG methods.

In the particle-hole symmetric case, the magnetic susceptibilities follow the universal curve at low temperatures. The local moment in the intermediate-temperature regime is suppressed in comparison of the $N=2$ case, which is mainly a consequence of the higher degeneracy. The Kondo temperatures, extrapolated from the susceptibility curves, follow within 10% the estimates from the generalized semiempirical equation based on the high-temperature perturbational theory of Haldane. In the $N=4$ case, we found good agreement with T_K calculated by Lin and Hirsch.

The overall behavior of the single-particle spectral functions follow the predictions of NCA and NRG. The height of the central Kondo peak increases with increasing degeneracy, since the Kondo temperature also increases with degeneracy when the other parameters remain constant. The height of the side peaks scales with degeneracy as $1/N$, as predicted by Zhang and Lee. The position of the side peaks depends slightly upon degeneracy when the unrenormalized energy difference between underlying states remains constant. We associate this degeneracy-induced increased renormalization with the increase of the effective hybridization. Within the computational error, we found universal behavior in the spectral functions at low frequencies when $N=4$. For $N=2$, such universality had been previously shown by Silver *et al.*

In the asymmetric case, the magnetic susceptibility follows the universal curve at low temperatures. Because of higher degeneracy and strong hybridization, we did not observe a pronounced local moment of mixed-valence regime. The position of the Kondo peak in the spectral density moves toward positive frequencies as the impurity energy increases from its value at the symmetric case. This shift scales with the Kondo temperature and with the average impurity occupancy as well. The side peaks also shift as the impurity energy increases. Moreover, as the lowest-energy state on the impurity site changes from f^2 to f^1, the peak on the BIS side grows while the peak on the PES side diminishes because of different phase spaces for transitions $f^1\rightarrow f^0$ and $f^1\rightarrow f^2$.

In conclusion, we established that the QMC and maximum-entropy methods give reliable results in the case of higher symmetry. However, higher degeneracy leads to larger fluctuations in the Monte Carlo data. Therefore, to obtain data of sufficient accuracy at higher

degeneracies, we had to increase the number of the Monte Carlo steps. These calculations require considerable computer time.

In the future, we intend to investigate the effect of the crystal-field and spin-orbit splittings on the spectral functions for the case of $N=6$. Special focus will be devoted to the effect of the splittings on the Kondo peak. Another line of future work will be to move the simulation to a massively parallel computer, which will enable us to investigate higher degeneracies, plus crystal-field and spin-orbit splittings, in order to model the physical systems even more closely. This move would enable us to calculate with improved statistics spectral properties based on the two-particle Green's function, such as the frequency-dependent magnetic susceptibility.

ACKNOWLEDGMENTS

This work was supported by the U.S. Department of Energy. We acknowledge helpful discussions with A. Arko, M. Jarrell, and J. W. Wilkins. We also thank S. W. Hodson and K. H. Winkler for making their workstation cluster available.

*Permanent address: J. Stefan Institute, University of Ljubljana, 61111 Ljubljana, Slovenia.

[1]P. W. Anderson, Phys. Rev. **124**, 41 (1961).

[2]A. M. Tsvelik and P. B. Wiegmann, Adv. Phys. **32**, 453 (1983).

[3]H. R. Krishna-murty, J. W. Wilkins, and K. G. Wilson, Phys. Rev. B **21**, 1003 (1980); **21**, 1044 (1980).

[4]L. N. Oliveira and J. W. Wilkins, Phys. Rev. B **24**, 4863 (1981).

[5]H. O. Frota and L. N. Oliveira, Phys. Rev. B **33**, 7871 (1986).

[6]O. Sakai, Y. Shimizu, and T. Kasuya, J. Phys. Soc. Jpn. **58**, 3666 (1989).

[7]N. E. Bickers, D. L. Cox, and J. W. Wilkins, Phys. Rev. B **36**, 2036 (1987); N. E. Bickers, Rev. Mod. Phys. **59**, 845 (1987). For alternative approaches to the large-degeneracy expansion, see, for example, O. Gunnarsson and K. Schönhammer, Phys. Rev. B **28**, 4315 (1983); N. Read and D. M. Newns, J. Phys. C **16**, 3273 (1982).

[8]J. W. Allen, Adv. Phys. **35**, 275 (1986).

[9]J. J. Joyce *et al.*, Phys. Rev. Lett. **68**, 236 (1992).

[10]R. N. Silver, D. S. Sivia, J. E. Gubernatis, and M. Jarrell, Phys. Rev. Lett. **65**, 496 (1990).

[11]J. E. Hirsch and R. M. Fye, Phys. Rev. Lett. **56**, 2521 (1986).

[12]P. Schlottmann, Z. Phys. B **51**, 49 (1983).

[13]H. Q. Lin and J. E. Hirsch, Phys. Rev. B **37**, 1864 (1988).

[14]G. D. Mahan, *Many-Particle Physics* (Plenum, New York, 1983), Chap. 3.

[15]R. Blackenbecler, D. J. Scalapino, and R. L. Shugar, Phys. Rev. D **24**, 2278 (1981).

[16]D. C. Langreth, Phys. Rev. **150**, 516 (1966).

[17]J. Holm and K. Shönhammer, Solid State Commun. **69**, 969 (1989).

[18]H. Keiter and Q. Qin, Physica B **163**, 594 (1990); H. Keiter and Q. Qin, Z. Phys. **79**, 397 (1990).

[19]J. E. Gubernatis, R. N. Silver, and M. Jarrell, Phys. Rev. B **44**, 6011 (1991).

[20]R. K. Bryan, Eur. Biophys. J. **18**, 165 (1990).

[21]S. D. M. Haldane, J. Phys. C **11**, 5015 (1978).

[22]F. C. Zhang and T. K. Lee, Phys. Rev. B **30**, 1556 (1984).